

Fabrication of high-speed InP/InGaAs/InP DHBT with a new self-aligned metallization technique for reduced base resistance

Kwangsik Choi ^{a,*}, Daekyu Yu ^a, Kyungho Lee ^a, Bumman Kim ^a,
H. Zhu ^b, K. Vargason ^b, J.M. Kuo ^b, P. Pinsukanjana ^b, Y.C. Kao ^b

^a Department of Electrical Engineering, Pohang University of Science and Technology (POSTECH), San 31, Hyoja-dong, Nam-gu, Pohang, Gyeongbuk 790-784, Republic of Korea

^b Intelligent Epitaxy Technology (IntelliEPI), Inc. 1250E. Collins Boulevard, Richardson, TX 75081, USA

Received 14 March 2005; received in revised form 21 July 2006; accepted 22 July 2006

The review of this paper was arranged by C. Tu

Abstract

A new self-aligned emitter–base metallization (SAEBM) technique with wet etch is developed for high-speed heterojunction bipolar transistors (HBTs) by reducing extrinsic base resistance. After mesa etch of the base layer using a photo-resist mask, the base and emitter metals are evaporated simultaneously to reduce the emitter–base gap (S_{EB}) and base gap resistance (R_{GAP}). The InP/InGaAs/InP double heterojunction bipolar transistor (DHBT) fabricated using the technique has a reduced R_{GAP} , from 16.48 Ω to 4.62 Ω comparing with the DHBT fabricated by conventional self-aligned base metallization (SABM) process. Furthermore, we adopt a novel collector undercut technique using selective etching nature of InP and InGaAs to reduce collector–base capacitance (C_{CB}). Due to the reduced R_{GAP} , the maximum oscillation frequency (f_{max}) for a 0.5 μm -emitter HBT is improved from 205 GHz to 295 GHz, while the cutoff frequency (f_T) is maintained at around 300 GHz.

© 2006 Elsevier Ltd. All rights reserved.

Keywords: Heterojunction bipolar transistors; Self-aligned base metallization; Base resistance; High-speed devices

1. Introduction

The operation frequency of transistors has been pushed steadily into higher frequencies due to the demand for high-speed circuits. To achieve a high cutoff frequency (f_T) and maximum oscillation frequency (f_{max}), which are the figures of merit for high-speed performance, the HBT design must achieve low base and collector transit times for high f_T ; balance between collector transit time, breakdown voltage and collector–base capacitance (C_{CB}); minimize the base resistance (R_B); minimize the extrinsic C_{CB} ;

and minimize the emitter contact resistance (R_E). C_{CB} and R_B especially are important factors for high f_{max} since $f_{max} \simeq \sqrt{f_T/8\pi R_B C_{CB}}$. Much research work has been devoted to reduce C_{CB} and R_B . To reduce C_{CB} , ion implantation [1,2] and undercut techniques are widely used [3,4]. Another solution to reduce C_{CB} is scaling the device laterally [5,6]. To reduce R_B , the base layer is thick and heavily doped. The doping concentration, however, is limited to $8 \times 10^{19} \text{ cm}^{-3}$ for p-type InGaAs by epitaxial growth technology, and the thickness cannot be too thick, which is limited by base transit time. Regrown base [6] and L-shaped electrodes [7] for reduced R_B have also been introduced. R_B is composed of intrinsic base resistance (R_{BI}), base contact resistance (R_{CONT}), and base gap resistance (R_{GAP}). R_{BI} can be controlled by vertical and lateral scaling. R_{CONT} is minimized by optimized metal composition, for example,

* Corresponding author. Tel.: +82 54 279 5584; fax: +82 54 279 8115.
E-mail addresses: torisis@postech.ac.kr (K. Choi), bestee@postech.ac.kr (K. Lee).

URL: www.postech.ac.kr/ee/mmic (K. Lee).

Pt for p-type InGaAs, but it cannot be scaled. R_{GAP} can be minimized by reducing the distance between emitter and base metal. Dry etching of the emitter cap and emitter layer can create a short-distance gap by its anisotropic nature. However, due to base layer damage by ion bombardment, high cost, and complexity such as after-treatment of byproduct from the CH_4/H_2 based reaction, dry etching has not been widely used. In case of selective wet etch of InP and InGaAs, which is most popularly used, it is very difficult to scale down the gap distance (S_{EB}) because of the isotropic etching nature of the InGaAs emitter cap layer.

In this paper, a new self-aligned emitter–base metallization (SAEBM) technique is proposed to reduce R_{GAP} by creating a short distance gap. Differently from the conventional self-aligned base metallization (SABM), which uses the emitter contact as an etch mask, photo-resist is used in the emitter definition. The final emitter geometry is determined by the controlled lateral etch depth (nearly isotropic) of InGaAs and InGaAlAs graded emitter cap layer. Subsequent InP emitter etch, which is anisotropic and intact to InGaAs, can make an optimized emitter undercut with a short gap distance (80 nm). For external interconnect, the problem of lowered height of the emitter contact is surmounted by our well-developed emitter-metal widening using polyimide. Additionally, the polyimide provides passivation of the emitter sidewall and extrinsic base with reduced surface leakage [8]. It also removes the risk of shorting between the emitter and base contacts. A novel collector undercut technique with selective etching nature of InP and InGaAs to reduce collector–base capacitance (C_{CB}) is also employed. Finally, we could significantly improve f_{max} by virtue of reduced R_{GAP} .

2. Device structure and fabrication

The epitaxial layers of the fabricated DHBTs are grown by IntelliEPI using Solid Source Molecular Beam Epitaxy (SSMBE) on an Fe-doped semi-insulating (100) InP sub-

strate. The emitter structure includes a InGaAs emitter cap layer (1000 Å) for low contact resistivity, a graded InGaAlAs layer (200 Å) for smoothing of band discontinuity, a highly doped InP cap layer (900 Å) for emitter undercut, and an InP emitter (700 Å, $7.0 \times 10^{17} \text{ cm}^{-3}$). The base layer is highly doped to $8 \times 10^{19} \text{ cm}^{-3}$ to obtain a low base sheet resistance. To achieve high β and reduce base transit time, the composition of the base layer is linearly graded from $x = 0.46$ to 0.53 toward collector, and the base layer is thin, 250 Å. To remove the carrier blocking effect due to conduction band discontinuity between InGaAs (base) and InP (collector), a linearly compositional graded $\text{In}_x\text{Ga}_y\text{Al}_{1-x-y}\text{As}$ layer (300 Å) is employed at the collector. Additionally, to compensate the reverse electric field induced by the graded layer, a delta-doped InP layer (30 Å, $1 \times 10^{18} \text{ cm}^{-3}$) is introduced within the collector layer [9]. The InP collector layer is doped to $2 \times 10^{16} \text{ cm}^{-3}$ and is thick, 1000 Å. Sub-collector layers are suitably designed for the undercut process explained in [10]. The whole layer structure is shown in Table 1.

Fig. 1(a) shows the conventional processes using SABM for InP-based DHBTs. In the process, the emitter mesa is etched laterally during etching of InGaAs and graded InGaAlAs emitter cap layer, and the space (S_{EB}) between the emitter mesa and base metal is widened. The widened S_{EB} increases R_{GAP} because the resistance is proportional to S_{EB} . Thin emitter can be a solution to avoid the lateral etching of the emitter mesa, and sidewall processes are also employed to prevent the connection between emitter and base metals [11]. In our new SAEBM technique, the emitter mesa is etched using the PR mask of emitter patterns at first. After removing the PR pattern, metallization process is followed for both emitter and base contacts simultaneously with Pt/Ti/Pt/Au. When the emitter mesa is formed in the $[01\bar{1}]$ crystal direction, the mesa has a shape of trapezoid. Because the thickness of emitter and emitter cap layer is thick and the shape of emitter mesa is an inverted trapezoid, the emitter and base metal contacts are formed safely without connection between the emitter

Table 1
Epitaxial layer structure of fabricated InP/InGaAs/InP DHBTs

Layer number	Material	Thickness (Å)	Concent. (cm^{-3})	Dopant	Carrier type
14	$\text{In}_{0.53}\text{Ga}_{0.47}\text{As}$	1000	3.0×10^{19}	Si	N+
13	$\text{In}_{(x)}\text{Ga}_{(y)}\text{Al}_{(1-x-y)}\text{As}$ grading	200	3.0×10^{19}	Si	N+
12	InP	900	1.0×10^{19}	Si	N+
11	InP	700	7.0×10^{17}	Si	N
10	$\text{In}_{0.46}\text{Ga}_{0.54}\text{As}$	20	Undoped		i
9	$\text{In}_{(x)}\text{Ga}_{(1-x)}\text{As}$ grading	250	8.0×10^{19}	C	P+
8	$\text{In}_{0.53}\text{Ga}_{0.47}\text{As}$	200	2.0×10^{16}	Si	N
7	$\text{In}_{(x)}\text{Ga}_{(y)}\text{Al}_{(1-x-y)}\text{As}$ grading	300	2.0×10^{16}	Si	N
6	InP	30	1.0×10^{18}	Si	N+
5	InP	1000	2.0×10^{16}	Si	N
4	InP	200	1.0×10^{19}	Si	N+
3	$\text{In}_{0.53}\text{Ga}_{0.47}\text{As}$	3000	3.0×10^{19}	Si	N+
2	InP	100	1.0×10^{19}	Si	N+
1	$\text{In}_{0.53}\text{Ga}_{0.47}\text{As}$	3000	3.0×10^{19}	Si	N+
0	Semi-insulating InP substrate				

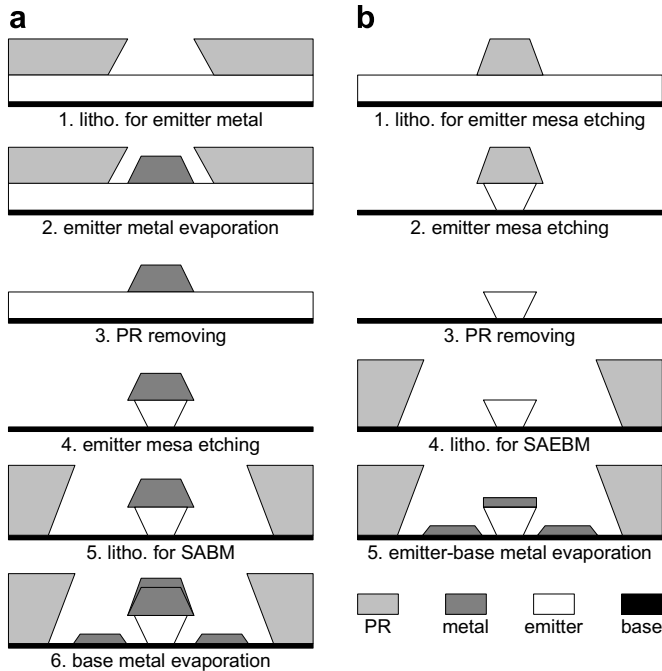


Fig. 1. Process flow of (a) conventional process using SABM and (b) new process using SABEM.

and base metals. A schematic of the new process flow is depicted in Fig. 1(b). When the conventional SABM process is used, S_{EB} is about 250 nm as shown in Fig. 2(a). If the SAEBM process is used, S_{EB} of 80 nm is expected from Fig. 2(a). Fig. 2(c) is the SEM picture after SAEBM

process. Fig. 2(b) and (d) show a schematic of SABM and SAEBM processes, respectively. In Fig. 2(d), S_{EB} is confirmed to be reduced to about 80 nm, below 100 nm. Because the emitter metal is deposited after the emitter mesa etching at the SAEBM, the lateral etching of the emitter mesa does not affect the space between the emitter mesa and base contact metal. This considerable reduction of S_{EB} is an advantage of the SAEBM technique. Besides, the SAEBM process is simpler than the SABM process.

Two types of InP/InGaAs/InP DHBTs are fabricated using the conventional SABM technique, called DHBT-C, and the new SAEBM technique, called DHBT-N with the same mask after base contact metallization. The emitter pattern is 0.8 μm , forming effectively 0.5 μm emitter, for both DHBTs. The collector undercut process is carried out as shown in Fig. 3(a)–(c). The emitter is protected by photo-resist pattern formed by a base contact mask and the base and collector layers are then etched with a citric acid-based and a hydrochloric acid-based etchant. After the base and collector layer etch, the emitter and base–collector mesas are protected by photo-resist. Then, the first InGaAs sub-collector is etched by a citric acid-based solution. By over-etch selectively from the InP etch stopper and collector layers, the InGaAs sub-collector under the InP collector is etched laterally and undercut (Fig. 3(a)). After that, the unveiled InP collector and InP etch stopper are etched by hydrochloric acid-based etchant (Fig. 3(b)). The SEM picture after the undercut process of DHBT-C is shown in Fig. 3(c). For interconnection to pads, the problems relating to the lower height of the emitter contact

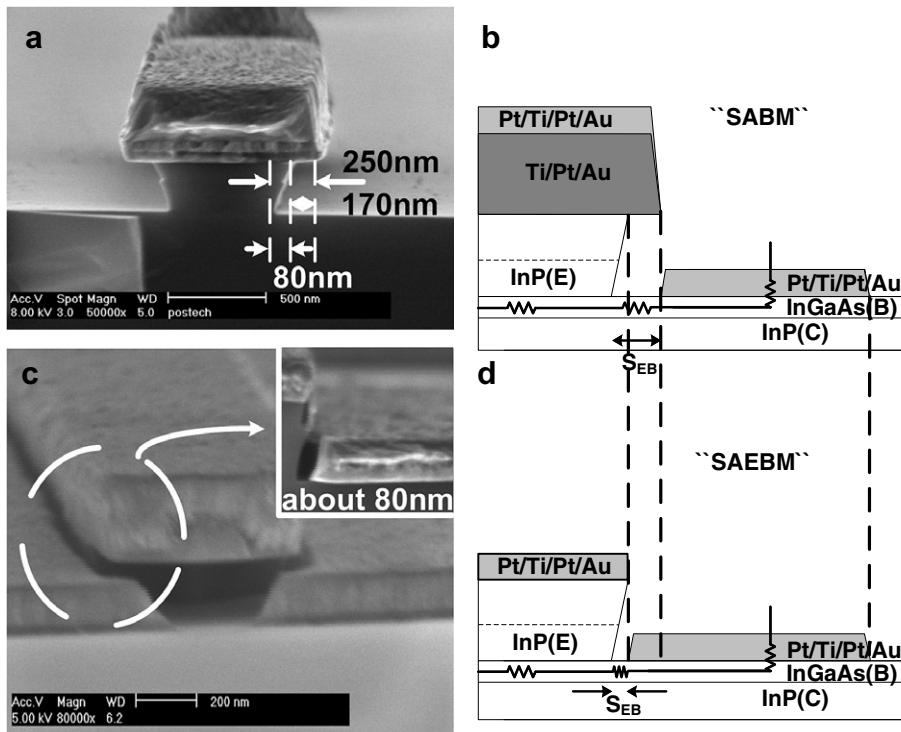


Fig. 2. (a) SEM picture after emitter mesa etching using conventional wet etching, (b) schematic of SABM process, (c) SEM picture after SAEBM process and (d) schematic of SAEBM process.

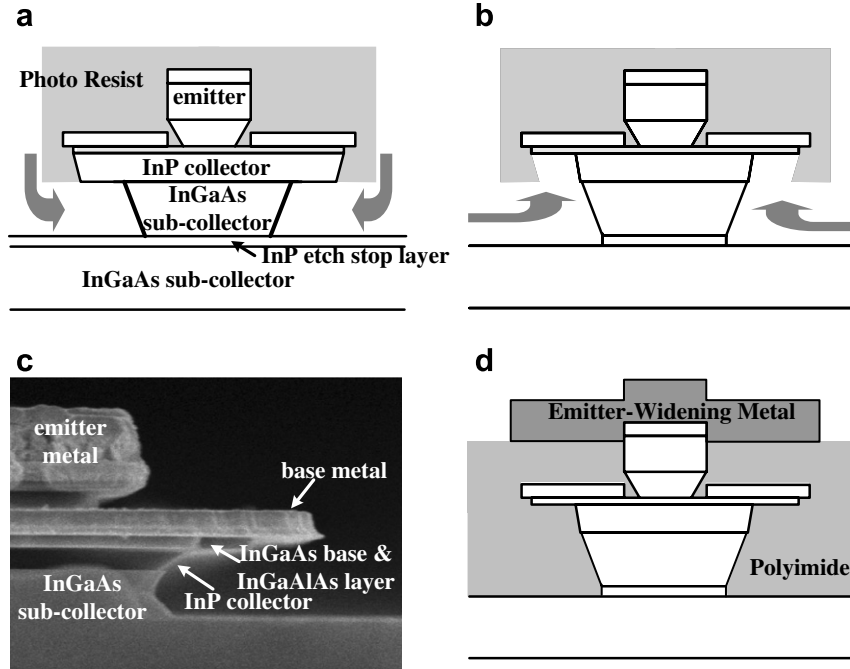


Fig. 3. Major unit processes; (a) collector undercut: over etching InGaAs sub-collector using citric-based etchant, (b) collector undercut: etching InP collector using hydrochloric acid-based etchant, (c) collector undercut: SEM picture and (d) emitter metal widening using polyimide planarization.

is overcome with our well-developed emitter-metal widening using polyimide. The polyimide is coated and then flatly etched without mask using O_2 RIE until the emitter metal is exposed, which can be controlled very accurately with a monitoring pattern. Next, a Ti/Au emitter widening metal is evaporated (Fig. 3(d)). Additionally, the polyimide provides passivation of the emitter sidewall and extrinsic base for reduced surface leakage, and it also eliminates the risk of shortening between the emitter and base contacts. A comprehensive process sequence can be found in our previous work [12].

3. Results and discussion

Normally, the emitter metal is composed of Ti/Pt/Au for the highly doped n-type InGaAs emitter cap layer, but the emitter metal is changed to base metal, because the base resistance is a critical factor for high-speed performance. Nevertheless, the specific contact resistivity of the emitter layer, measured using transmission line measurement (TLM), is $1.8 \times 10^{-8} \Omega \text{ cm}^2$ for DHBT-N, which is quite low.

The measured common emitter I - V curves of the fabricated DHBTs with $0.5 \times 6 \mu\text{m}^2$ emitter area are depicted in Fig. 4. The dc current gain (β) of DHBT-C and DHBT-N are about 30 and 25, respectively. The breakdown voltage of two devices at an open base, BV_{CEO} , is similar, around 6.2 V at $100 \mu\text{A}$ collector current. The difference of β between DHBT-C and DHBT-N can be explained by analysis of the base current, composed of surface recombination current (J_{SURF}), contact recombination current (J_{CONT}), bulk recombination current (J_{BULK}), space-

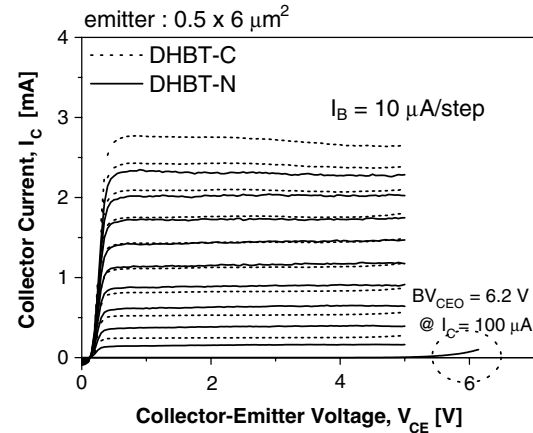


Fig. 4. Common emitter I_C - V_{CE} characteristics under forced constant base currents.

charge recombination current (J_{SCR}), and back-injected hole current (J_{BP}). With the periphery dependence of J_{SURF} and J_{CONT} and the area dependence of the others, J_C/β is expressed by

$$\frac{J_C}{\beta} = J_{\text{BULK}} + J_{\text{SCR}} + J_{\text{BP}} + 2 \cdot (J_{\text{SURF}} + J_{\text{CONT}}) \cdot \left(\frac{1}{W_E} + \frac{1}{L_E} \right) \quad (1)$$

where J_C is collector current density. J_C/β is measured as a function of $(1/W_E + 1/L_E)$ and depicted in Fig. 5. For the linear fitting curves of $J_{\text{SURF}} + J_{\text{CONT}}$, DHBT-N is higher than DHBT-C at both $J_C = 1 \times 10^4 \text{ A/cm}^2$ and $J_C = 5 \times 10^4 \text{ A/cm}^2$. Since the surface recombination current

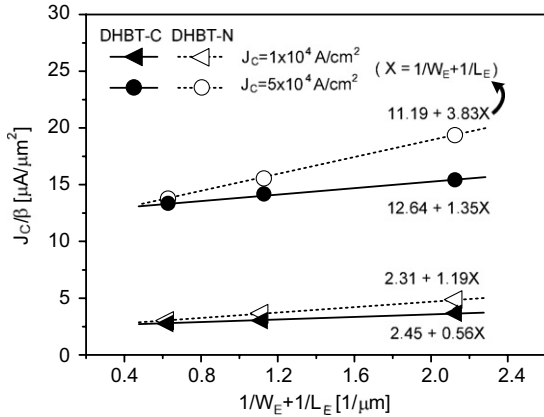


Fig. 5. J_C/β versus $(1/W_E + 1/L_E)$ characteristics for DHBT-C (filled) and DHBT-N (empty) at $J_C = 1 \times 10^4 \text{ A/cm}^2$ and $J_C = 5 \times 10^4 \text{ A/cm}^2$. Emitter sizes used: $0.5 \times 6 \mu\text{m}^2$, $1 \times 6 \mu\text{m}^2$, and $2 \times 6 \mu\text{m}^2$.

can be neglected for p-type InGaAs with low surface recombination velocity, this increased periphery dependent currents are caused by increased base contact recombination current due to the relatively short gap distance of DHBT-N [13]. Therefore, DHBT-N has a smaller β than DHBT-C.

Microwave performance is characterized by on-wafer S-parameter measurements from 0.5 to 40 GHz using a HP8510C vector network analyzer. Fig. 6 shows the frequency dependence of current gain $|H_{21}|^2$, G_{max} (MSG/MAG), Mason's unilateral gain, and stability factor (k) for both DHBTs at similar bias points. DHBT-N has a lower k than DHBT-C due to the reduced base resistance and is more unstable. The f_T and f_{max} are obtained assuming a -20 dB/decade frequency dependence of the current gain and Mason's unilateral gain, respectively. For DHBT-C, $f_T = 275 \text{ GHz}$ and $f_{\text{max}} = 206 \text{ GHz}$ are obtained at $J_C = 363 \text{ kA/cm}^2$ and $V_{\text{CE}} = 1.5 \text{ V}$. For DHBT-N, $f_T = 290 \text{ GHz}$ and $f_{\text{max}} = 296 \text{ GHz}$ are obtained at $J_C = 385 \text{ kA/cm}^2$ and $V_{\text{CE}} = 1.5 \text{ V}$. Since the base resistance

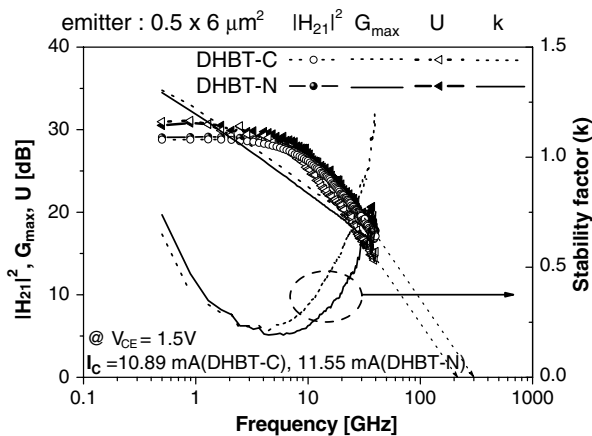


Fig. 6. Frequency dependencies of $|H_{21}|^2$, G_{max} (MSG/MAG), Mason's gain U , and stability factor (k) for fabricated DHBTs as determined by S-parameter measurements at $V_{\text{CE}} = 1.5 \text{ V}$ and $I_C = 10.89 \text{ mA}$ (DHBT-C), 11.55 mA (DHBT-N).

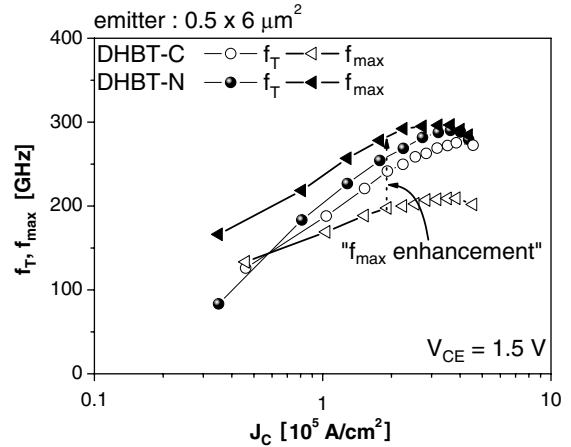


Fig. 7. Dependencies of f_T and f_{max} on collector current density for DHBT-C and DHBT-N at $V_{\text{CE}} = 1.5 \text{ V}$.

does not affect the transit time significantly, f_T 's of the two DHBTs are similar. However, the f_{max} of DHBT-N is improved about 90 GHz by using the SAEBM technique. Fig. 7 shows the dependence of f_T and f_{max} on collector current density for both devices.

We have analyzed R_B further using the following relationships:

$$R_B = R_{\text{BI}} + R_{\text{CONT}} + R_{\text{GAP}} \quad (2)$$

$$R_{\text{BI}} = \frac{1}{12} \cdot R_{\text{SH,B}} \cdot \frac{W_E}{L_E} \quad (3)$$

$$R_{\text{GAP}} = \frac{1}{2} \cdot R_{\text{SH,B}} \cdot \frac{S_{\text{EB}}}{L_E} \quad (4)$$

$$R_{\text{CONT}} = \frac{1}{2} \cdot \frac{\sqrt{R_{\text{SH,B}} \cdot \rho_{\sigma\text{B}}}}{L_E} \cdot \coth \left(W_B \cdot \sqrt{\frac{R_{\text{SH,B}}}{\rho_{\sigma\text{B}}}} \right) \quad (5)$$

where $R_{\text{SH,B}}$ is base sheet resistance, W_E and W_B are emitter and base widths, respectively, L_E is emitter length, similar to base length, S_{EB} and $\rho_{\sigma\text{B}}$ are base gap distance and base specific contact resistivity, respectively. The $R_{\text{SH,B}}$ and $\rho_{\sigma\text{B}}$ of base layer are $790 \Omega/\square$ and $2.4 \times 10^{-7} \Omega \text{ cm}^2$, respectively, for both DHBTs. The transfer length, L_T , expressed as $\sqrt{\rho_{\sigma\text{B}}/R_{\text{SH,B}}}$, is $0.4 \mu\text{m}$ and the base contact resistance is maintained low. Table 2 lists the calculated base resistances for both DHBTs. To verify the reduced base resistance, small-signal model parameters of the two devices with $0.5 \times 6 \mu\text{m}^2$ emitter geometry are extracted directly using our method [14] at maximum f_{max} bias point and listed in Table 3. Most of the extracted parameters are identical

Table 2
Calculated base resistances of DHBT-C and DHBT-N with $0.5 \times 6 \mu\text{m}^2$ emitter area

	$R_{\text{BI-cal}} (\Omega)$	$R_{\text{BX-cal}} (\Omega)$	
		R_{CONT}	R_{GAP}
DHBT-C	5.49	11.49	16.48
DHBT-N	5.49	11.49	4.62

Table 3
Extracted small signal model parameters of DHBT-C and DHBT-N with $0.5 \times 6 \mu\text{m}^2$ emitter area

	R_{ex} (Ω)	R_{bi} (Ω)	R_{bx} (Ω)	g_{m} (ms)	r_{π} (Ω)	C_{π} (pF)	C_{cbi} (fF)	C_{cbx} (fF)
DHBT-C	8.49	4.79	28.11	0.45	67.1	0.19	2.55	5.42
DHBT-N	7.27	5.11	15.10	0.42	62.2	0.17	2.50	5.38

for the two devices except R_{bx} , 28.11 Ω for DHBT-C and 15.10 Ω for DHBT-N. The difference of R_{bx} between DHBT-C and DHBT-N is the result of reduced S_{EB} , that is, reduction of R_{GAP} . Since S_{EB} is reduced from 250 nm to 80 nm from the SEM picture, R_{GAP} is reduced from 16.48 Ω to 4.62 Ω , estimated using Eq. (4), about 72% reduction of R_{GAP} . This reduction is about 39% of the total base resistance of DHBT-C. This data show clearly that SAEBM is a very effective technique to enhance f_{max} .

4. Conclusion

A new but simple SAEBM technique with wet etch has been developed to improve the high-speed performance, especially f_{max} , of HBTs. Using the SAEBM technique for InP-based DHBTs, R_{GAP} is reduced from 16.48 Ω to 4.62 Ω and f_{max} is improved about 90 GHz without any degradation of f_{T} . High frequency performance of $f_{\text{T}} = 290$ GHz and $f_{\text{max}} = 296$ GHz is obtained for a $0.5 \times 6 \mu\text{m}^2$ DHBT-N with $\text{BV}_{\text{CEO}} = 6.2$ V. The RF performance results demonstrate the effectiveness of the new SAEBM technique for enhanced performance. Further improvements of f_{max} and f_{T} are expected by lateral scaling in the geometrical layout and parasitic reductions. Furthermore, if the emitter mesa etching is controlled precisely, nano-scale HBTs can be fabricated using the SAEBM technique without using e-beam lithography.

Acknowledgements

This work was supported in part by the Korean Ministry of Education under BK21 project and the center for Broadband OFDM Mobile Access (BrOMA) at POS-TECH through the ITRC program of the Korean MIC, supervised by IITA (IITA-2005-C1090-0502-0008).

References

- [1] Ho MC, Johnson RA, Ho WJ, Chang MF, Asbeck PM. High-performance low-base-collector capacitance AlGaAs/GaAs heterojunction bipolar transistors fabricated by deep ion implantation. *IEEE Electron Dev Lett* 1995;16(11):512–4.
- [2] Li JC, Chen M, Hitko DA, Fields CH, Shi B, et al. A submicrometer 252 GHz f_{T} and 283 GHz f_{max} InP DHBT with reduced C_{BC} using selectively implanted buried subcollector (SIBS). *IEEE Electron Dev Lett* 2005;26(3):136–8.
- [3] Lee K, Yu D, Chung M, Kang J, Kim B. New collector undercut technique using a SiN sidewall for low base contact resistance in InP/InGaAs SHBTs. *IEEE Trans Electron Dev* 2002;49(6):1079–82.
- [4] Yu D, Choi K, Lee K, Kim B, Ontiveros D, et al. Realization of high-speed InP SHBTs using novel but simple techniques for parasitic reduction. *IEEE Int Conf Indium Phosphide Relat Mater (IPRM) 2004;Symp-2004:753–6*.
- [5] Rodwell MJW, Urteaga M, Mathew T, Scott D, Mensa D, et al. Submicron scaling of HBTs. *IEEE Trans Electron Dev* 2001;48(11):2606–24.
- [6] Shimawaki H, Amamiya Y, Furuhashi N, Honjo K. High- f_{max} AlGaAs/InGaAs and AlGaAs/GaAs HBTs with p+/p regrown base contacts. *IEEE Trans Electron Dev* 1995;42(10):1735–44.
- [7] Yanagihara M, Sakai H, Ota Y, Tanabe M, Inoue K, Tamura A. 253-GHz f_{max} AlGaAs/GaAs HBT with Ni/Ti/Pt/Ti/Pt-contact and L-shaped base electrode. *IEEE Int Electron Dev Meeting (IEDM) 1990; Dig-1990:807–10*.
- [8] Caffein E, Bricard L, Courant JL, How Kee Chun LS, Lescaut B, et al. Passivation of InP-based HBTs for high bit rate circuit applications. *IEEE Int Conf Indium Phosphide Relat Mater (IPRM) 1997;Symp-1997:637–40*.
- [9] Block TR, Wojtowicz M, Cowles J, Tran L, Oki AK, Streit DC. Molecular beam epitaxy growth and characterization of InGaAlAs-collector heterojunction bipolar transistors with 140 GHz f_{max} and 20 V breakdown. *J Vac Sci Technol* 1996;B14(3):2221–4.
- [10] Jeong Y, Song Y, Choi S, Yoon M, Yang K. f_{max} enhancement in InP-based DHBTs using a new lateral reverse-etching technique. *IEEE Int Conf Indium Phosphide Relat Mater 2003;Symp-2003:22–5*.
- [11] Urteaga M, Rierison R, Rowell P, Brar B, Griffith Z, et al. Wide bandwidth InP DHBT technology utilizing dielectric sidewall spacers. *IEEE Int Conf Indium Phosphide Relat Mater (IPRM) 2004;Symp-2004:667–70*.
- [12] Yu D, Lee K, Kim B, Ontiveros D, Vargason K, et al. Ultra high-speed InP/InGaAs SHBTs with f_{max} of 478 GHz. *IEEE Electron Dev Lett* 2003;24(6):384–6.
- [13] Liu W, Harris JS. Effects of emitter–base contact spacing on the current gain in heterojunction bipolar transistors. *Jpn J Appl Phys* 1992;31(8):2349–51.
- [14] Lee K, Choi K, Kook SH, Cho DH, Park KW, Kim B. Direct parameter extraction of SiGe HBTs for the VBIC bipolar compact model. *IEEE Trans Electron Dev* 2005;52(3):375–84.